DESY 15-060, SFB/CPP-14-125

Thermal evolution of the Schwinger model with Matrix Product Operators

M. C. Bañuls,[1] K. Cichy,[2,3,4] J. I. Cirac,[1] K. Jansen,[3] and H. Saito[3]

[1] *Max-Planck-Institut für Quantenoptik, Hans-Kopfermann-Str. 1, 85748 Garching, Germany*
[2] *Goethe-Universität, Institut für Theoretische Physik, Max-von-Laue-Straße 1, D-60438 Frankfurt a.M., Germany*
[3] *NIC, DESY, Platanenallee 6, D-15738 Zeuthen, Germany*
[4] *Adam Mickiewicz University, Faculty of Physics, Umultowska 85, 61-614 Poznan, Poland*

(Dated: May 5, 2015)

We demonstrate the suitability of tensor network techniques for describing the thermal evolution of lattice gauge theories. As a benchmark case, we have studied the temperature dependence of the chiral condensate in the Schwinger model, using matrix product operators to approximate the thermal equilibrium states for finite system sizes with non-zero lattice spacings. We show how these techniques allow for reliable extrapolations in bond dimension, step width, system size and lattice spacing, and for a systematic estimation and control of all error sources involved in the calculation. The reached values of the lattice spacing are small enough to capture the most challenging region of high temperatures and the final results are consistent with the analytical prediction by Sachs and Wipf over a broad temperature range.

PACS numbers: 11.15.Ha, 02.70.-c
Keywords: lattice gauge theory, Schwinger model, Hamiltonian approach, Matrix Product States, finite temperature

INTRODUCTION

Tensor network (TN) techniques have recently revealed their potential to study lattice gauge theories (LGT). Numerical studies have demonstrated that matrix product states (MPS) can accurately describe ground state and low excited levels of the Schwinger model [1–6] and of related quantum link models [7, 8], and tensor renormalization group methods have been used to evaluate the path integral [9, 10]. More generally, a framework has been proposed to construct gauge invariant TN states in higher dimensions [11, 12].

The TN ansatz can also be used to describe thermal equilibrium states. Non-zero temperature studies have played a major role in lattice QCD computations, establishing a crossover behavior of QCD in the early universe [13]. Such calculations will be very important in the future for understanding QCD matter, see [14]. Different from most LGT calculations, tensor network methods work in the Hamiltonian formalism. In this approach, it is in principle possible to follow the complete thermal evolution of the system. Thus, employing Hamiltonian calculations could allow us to map out the temperature dependence of many physical quantities over a much broader temperature regime and in a more precise way than conventional Markov Chain Monte Carlo methods.

In this work, we show that the matrix product operator (MPO) ansatz can accurately describe the thermal equilibrium states of the Schwinger model. To this end, we investigate the temperature dependence of the chiral condensate in the continuum limit for the massless case, for which analytical results were provided in [15]. Our results are consistent with the analytical prediction at all (dimensionless) inverse temperatures $g\beta \in [0, 6]$. Our lattice calculation using MPO requires a series of consecutive extrapolations. We describe how to carry out these steps and demonstrate that all systematic errors inherent to the method can be controlled and systematically improved. Thus, the procedure yields reliable continuum values and is applicable also when the exact value is completely unknown.

We use Gauss' law to integrate out the gauge degrees of freedom and apply TN states to describe the fermionic degrees of freedom in the exact physical subspace, as in [3, 4]. Here we demonstrate that this approach, initially presented in [16], is also suitable for thermal states. Alternatively, one could include both fermionic and bosonic degrees of freedom and impose gauge symmetry on the tensors, as in [1, 5–8], but in that case the gauge degrees of freedom need to be truncated, which introduces an additional extrapolation in the procedure, which also has to be taken into account in the systematic errors.

THE MODEL AND THE HAMILTONIAN SETUP

The Schwinger model [17] or QED in $1 + 1$ dimensions, is frequently used as a testbench for lattice calculations. In order to apply TN methods, we work in the Hamiltonian formalism (see e.g. [3]), which implies we have to impose Gauss' law as a constraint on physical states. The Kogut-Susskind Hamiltonian [18] can be mapped to a spin system by a Jordan-Wigner transformation [19]. Using Gauss' law, the gauge degrees of freedom can be eliminated [20], since the electric flux on a link is completely determined by the spin content and

the background field, so that the model can be written:

$$H = x\sum_{n=0}^{N-2}\left[\sigma_n^+\sigma_{n+1}^- + \sigma_n^-\sigma_{n+1}^+\right] + \frac{\mu}{2}\sum_{n=0}^{N-1}\left[1+(-1)^n\sigma_n^z\right] + \sum_{n=0}^{N-2}\left[\ell + \frac{1}{2}\sum_{k=0}^{n}((-1)^k+\sigma_k^z)\right]^2, \quad (1)$$

where ℓ is the boundary electric field (on the leftmost link), which can describe the background field, and the parameters of the model are $x = \frac{1}{g^2a^2}$, $\mu = \frac{2m}{g^2a}$, in terms of the lattice spacing, a, the fermion mass, m, and the coupling, g.

It is then possible to use a basis $|\ell\rangle|i_0 i_1 \dots i_{N-1}\rangle$ to describe the physical space. For finite systems, the value of ℓ is conserved. In the following, we will consider the case $\ell = 0$ and omit it from the basis. We focus on the temperature dependence of the chiral condensate, $\Sigma = \langle\bar{\Psi}\Psi\rangle/g$, which is the order parameter of the chiral symmetry breaking, and which in terms of spin operators reads $\Sigma = \frac{\sqrt{x}}{N}\sum_n(-1)^n\frac{1+\sigma_n^z}{2}$.

THE ANSATZ

An MPS for a system of N sites with internal dimension d and individual basis $\{|i\rangle\}_{i=1}^d$ is a state of the form $|\Psi\rangle = \sum_{i_0,\dots i_{N-1}=1}^{d}\mathrm{tr}(A_0^{i_0}\dots A_{N-1}^{i_{N-1}})|i_0,\dots i_{N-1}\rangle$, where each A_k^i is a D-dimensional matrix, and the bond dimension, D, determines the number of free parameters in the ansatz [21–23]. MPS are known to provide good approximations to ground states of local Hamiltonians in the gapped phase [24] and have also been successfully used for more general situations [25]. The analogous ansatz in the space of operators [26–28] is called matrix product operators (MPO), and can be used to efficiently approximate thermal states of local Hamiltonians [29, 30].

To find an MPO approximation to the Gibbs state, $\rho \propto e^{-\beta H}$, a Suzuki-Trotter decomposition is applied to the exponential, with the Hamiltonian split into several terms whose exponentials are easily written or approximated as MPO. In the case of Hamiltonian (1), it is convenient to split $H = H_e + H_o + H_z$, where $H_{e(o)}$ contains the $\sigma_n^+\sigma_{n+1}^- + h.c.$ terms for even (odd) n, and H_z contains the mass terms and the long range $\sigma_n^z\sigma_m^z$ interactions. The exponentials of $H_{e(o)}$ can be easily written as exact MPO [28]. For H_z, instead, the exponential can only be approximated. Adopting a 2nd-order Trotter expansion and, for H_z, a 1st-order Taylor expansion, we can write:

$$\rho(\beta) \approx \left[e^{-\frac{\delta}{2}H_e}\left(1-\frac{\delta}{2}H_z\right)e^{-\delta H_o}\left(1-\frac{\delta}{2}H_z\right)e^{-\frac{\delta}{2}H_e}\right]^M, \quad (2)$$

where $\delta = \beta/M$ is the step width, and the final error for fixed β will be $\mathcal{O}(\delta)$, dominated by the Taylor expansion.

Starting from the identity operator, which corresponds to infinite temperature, $\rho(\beta = 0)$, we apply successive Euclidean evolution steps. After each of them a truncation is carried out to find an MPO approximation to the result. To this end, using a Choi isomorphism, the MPO is mapped to an MPS with local physical dimension d^2, and an alternating least squares procedure is applied to minimize the Euclidean distance between the vectorized MPO for the new and evolved states. Since the truncation does not preserve the positivity of the whole state, it is more convenient to compute $\rho(\beta/2)^\dagger\rho(\beta/2)$, where the Trotter expansion explained above is used for each factor. [35]

RESULTS

To compute the chiral condensate in the infinite volume and continuum limits, we approximate the thermal state at each $g\beta \in [0, 6]$ over a range of values of $x \in [4, 65]$. For each value, we consider various system sizes, with $N/\sqrt{x} \in [16, 24]$ to ensure consistent physical volumes, and for each of them, different step widths, δ, and bond dimensions. We thus need to control effects of successively extrapolating in D, δ, N and x.

The limited bond dimension, D, used for each fixed set of values (x, N, δ) induces a systematic truncation error. The MPS family being complete, the results converge to the exact value for the given problem in the limit of very large D (of the order of the dimension of the operator space) [23]. From our finite D results, we estimate the final value of Σ as the one obtained for the largest achieved bond dimension, $D_{\max}$, and the error as the difference between this value and the one obtained from $D_{\max} - 20$, as illustrated in the left panel of Fig. 1.

A second source of systematic error is the finite step width, δ. Although we use a second order Suzuki-Trotter expansion, the Taylor approximation in (2) induces linear corrections, $\mathcal{O}(\delta)$. We can thus extrapolate linearly to obtain the value as $\delta \to 0$, as illustrated by the right panel in Fig. 1 for selected examples. Furthermore, the Taylor approximation requires that the value of δ employed in the calculation is below a certain threshold, to ensure convergence of the expansion. We find that values $\delta = 10^{-6}$-10^{-3} are sufficiently small for the considered values of x and N.

The previous steps yield a result for each pair (x, N). As in [3, 4], we then find the thermodynamic limit by fitting the results to a linear function in $1/N$. The left panel of Fig. 2 shows how accurately this extrapolation fits our results for the considered values of x.

From the infinite volume results for each lattice spacing at fixed $g\beta$, we can perform the continuum extrapolation. As we showed in [4], the condensate exhibits logarithmic corrections $\mathcal{O}(a\log(a))$. Hence we try two fitting functions, which additionally include linear or linear and

quadratic corrections in a,

$$f_1(x) = \Sigma_{\text{cont}} + \frac{a_1}{\sqrt{x}}\log(x) + \frac{b_1}{\sqrt{x}},$$
$$f_2(x) = \Sigma_{\text{cont}} + \frac{a_2}{\sqrt{x}}\log(x) + \frac{b_2}{\sqrt{x}} + \frac{c_2}{x}. \qquad (3)$$

To include the uncertainty from the choice of the functional form of the fitting ansatz, we finally take as central value the result from the fit to f_1, and as systematic error the difference between both. Fig. 3 demonstrates these fits for two very different temperatures, $g\beta = 0.4$ and 4.0, and shows that quadratic corrections will only be significant at lower temperatures. Higher order corrections do not provide any significant improvement for the fitting range $x \in [4, 65]$.

After performing for each value of $g\beta$ all the steps described above, we obtain for the chiral condensate the temperature dependence shown in Fig. 5. Comparing to the analytical result in [15], we find excellent agreement for all $g\beta \geq 0.5$. Although the central values lie very close to the exact results, the errors shown in Fig. 5 seem relatively large because they include the propagated errors from the extrapolations in D, δ, N and x, as well as the systematic error from the form of the fitting ansatz for the continuum extrapolation. Our approach makes it possible to fully control all sources of uncertainties. This rigorous account of errors is crucial to ensure that the technique can be used in a general situation, for which no analytical results are available.

Different kinds of errors contribute distinctly at different temperatures. For small $g\beta$, cut-off effects are enhanced, and systematic errors from the choice of the fitting ansatz can be an order of magnitude larger than other errors. Lowering the temperature, the effect becomes smaller, while other errors grow, in particular the propagated error from the $D \to \infty$ extrapolation. Interestingly, at intermediate values, $g\beta \approx 2$, the slope of the $N \to \infty$ extrapolations changes sign (see Fig. 2). Moreover, for this region of temperatures, the continuum limit extrapolations from f_1 and f_2 are very close. For larger $g\beta$, all errors grow, but the increase is faster for D and δ extrapolations so that at the end of our $g\beta$ range they are an order of magnitude larger than the systematic error from the choice of the fitting ansatz.

The approach is systematically improvable, because it is clear how to reduce each uncertainty. For the present analysis, the relatively most important error comes from the extrapolation in D. We chose a rather conservative criterion to estimate this error and it is natural to expect that much more accurate results can be obtained by checking the convergence in bond dimension with larger values of D. The cost of the computation scales with D^3, which makes the scan over a rather broad range of D feasible. It is nevertheless remarkable that the very accurate results presented here were obtained with a relatively small $D \leq 100$. This shows how adequate the MPO ansatz is for thermal states in this gauge theory.

For the region of very small $g\beta$, we find a significant deviation from the analytical results (see Fig. 5), although the individual points at finite x are accurate enough, because much smaller lattice spacings are required in order to correctly capture the asymptotic behavior. Using the procedure described above, it is possible to reach larger values of x, by incurring a higher computational cost, since the required system size grows as $\sqrt{x}$ to maintain a consistent physical volume, and correspondingly the threshold δ that ensures convergence decreases.

Using an alternative approximation for the exponential of H_z that avoids the Taylor expansion, it is however possible to explore the region of larger x at a lower computational cost. Indeed, $e^{-\delta H_z}$ can be written exactly as an MPO of bond dimension $\mathcal{O}(N)$. For systems of several hundreds of sites this is unpractical, but this exponential can be approximated by projecting out those spin configurations that correspond to an electric flux larger than a certain cutoff, L_{cut}, on any of the links. This results in an MPO with bond dimension $2L_{\text{cut}} + 1$. Notice that this truncation is equivalent to limiting the maximum occupation number for the bosonic degrees of freedom, as done in [1, 5, 6] for pure states. However, the latter results in twice as large system sizes, since bosonic degrees of freedom are kept explicitly, and, in principle, in local dimensions that scale as $(2L_{\text{cut}} + 1)^2$ for the additional sites in the MPO. [36]

Although the cost of applying the MPO for the projected exponential is higher than that of the Taylor approximation, the step width error is now $\mathcal{O}(\delta^2)$, determined by the second order Trotter expansion, and there is no threshold value for δ, which allows us to reach the same $g\beta$ with fewer steps. To explore the small $g\beta$ region, we study the range $x \in [4, 1024]$. For each value of x, we compute different system sizes, step widths and L_{cut} values, and for each of them bond dimensions up to $D = 160$. As described above, we successively extrapolate $1/D \to 0$ (as before), $\delta \to 0$ (linear in δ^2) and $1/N \to 0$, as illustrated by Fig. 4 (left). To account for the additional systematic error due to the cutoff parameter, we can also extrapolate in L_{cut}. However, comparing the results for $L_{\text{cut}} \in [5, 15]$, we observe (see Fig. 4) that the effect is very small, and results for $L_{\text{cut}} \geq 8$ are compatible within our numerical precision (inset of Fig. 4 right), so here we present the results for $L_{\text{cut}} = 10$ and leave the detailed analysis of the cutoff effects to a more technical work [31].

This relatively small L_{cut} allows us to study the lattice effects for the smallest $g\beta$. As shown in Fig. 4, $g\beta = 0.1$ requires $x \approx 300$ or larger to obtain an accurate continuum extrapolation. We observe that higher order corrections are present and adopt as central value the result of the fit $f_3(x) = \Sigma_{\text{cont}} + \frac{a_3}{\sqrt{x}}\log(x) + \frac{b_3}{\sqrt{x}} + \frac{c_3}{x} + \frac{d_3}{x\sqrt{x}}$ [37] and we estimate the error from using different fitting

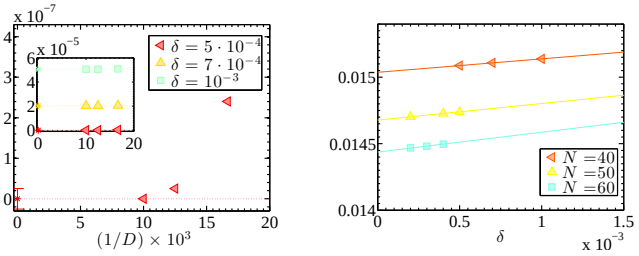

FIG. 1: Left: convergence of condensate value with bond dimension, D, for $g\beta = 0.4$, $x = 6.25$, $N = 40$ and $\delta = 5 \cdot 10^{-4}$. Shown is the deviation with respect to the final value, $\Sigma = 0.01508769$. Looking at various δ (inset) we find that the truncation error is much smaller than the variation due to the finite step width. Right: linear δ extrapolation for the same x and $g\beta$ and several system sizes.

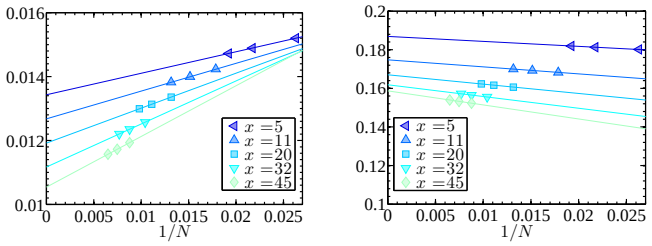

FIG. 2: Infinite volume extrapolation of the condensate values for several values of x at $g\beta = 0.4$ (left) and 4.0 (right).

ranges. Notice that to properly deal with the uncertainty due to the fit, we could run a statistical analysis as was done in [3], but the simple estimate used here allows us to appreciate the relevance of reaching large x values.

Finally, we obtain for the temperature dependence of the chiral condensate the improved results shown in Fig. 5 (right), consistent with the analytical result at high temperatures.

CONCLUSION

Using the massless Schwinger model as a benchmark, we have demonstrated that finite Matrix Product Operators can successfully describe thermal equilibrium states of lattice gauge theories. We have evaluated the thermal evolution of the chiral condensate in this model and found good agreement with the analytical result [15] from infinite to almost zero temperature.

The high temperature region is the hardest one to capture in the continuum limit, maybe counterintuitively, since for typical condensed matter models it is easier to describe. On the other hand, it is known that lattice spacing effects in the high temperature region can be non-negligible in conventional lattice simulations. We have nevertheless shown that using the MPO ansatz, it is also possible to obtain precise results at very small lattice

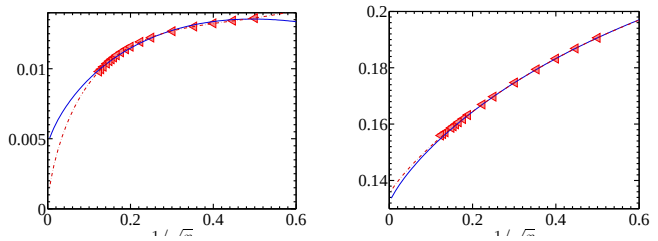

FIG. 3: Condensate, Σ, as a function of the lattice spacing for $g\beta = 0.4$ (left) and 4.0 (right). The lines show the continuum extrapolation using f_1 (solid blue) and f_2 (dash-dotted red).

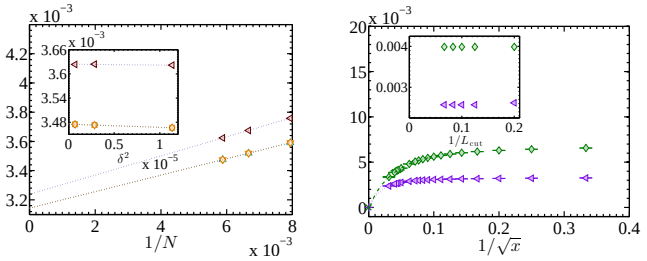

FIG. 4: Condensate values with a truncation $L_{\rm cut}$ of the maximum electric flux per link. Left: finite volume extrapolation for $x = 55$, $g\beta = 0.1$ from $L_{\rm cut} = 5$ (left pointing red triangles), 8, 10, 12 (different shapes and colors, indistinguishable in the plot) and 15 (orange diamonds). The inset shows the extrapolation in Trotter parameter, δ, for $N = 170$ and $L_{\rm cut} = 8 - 15$. Right: continuum limit for $g\beta = 0.1$ (left pointing purple triangles) and 0.2 (green diamonds). The corresponding exact results from [15] are indicated on the vertical axis. The inset shows explicitly the dependence on the cutoff for these $g\beta$ values at $x = 55$.

spacings.

Our approach offers a systematic procedure to evaluate and control all systematic errors in the calculation, namely bond dimension of the ansatz, step width of the Trotter expansion for the exponential operators, finite volume and continuum limit. Although not strictly necessary, a truncation of the maximum electric flux per link can be introduced to enhance the numerical performance. The effect of this additional cutoff parameter is very small, but can equally be taken into account in the systematic error analysis.

All this makes the MPS and MPO ansätze most valuable and promising tools to evaluate also other one-dimensional Hamiltonian systems relevant for gauge field theories. The most interesting open question is the extension of these techniques to higher dimensions.

Acknowledgments. We are grateful to B. Buyens, S. Kühn, M. Lubasch and K. Van Acoleyen for discussions. This work was partially funded by the EU through SIQS grant (FP7 600645), and by the DFG Sonderforschungsbereich/Transregio SFB/TR9. K.C. has been supported in part by the Helmholtz International Center for FAIR within the framework of the LOEWE program

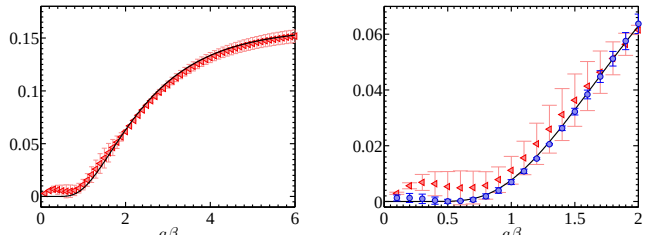

FIG. 5: Temperature dependence of the chiral condensate from data with $x \leq 65$ and exact gauge sector (red triangles), compared to [15] (solid line). For the lowest $g\beta$ (right), the results deviate from the exact ones. Using the $L_{\text{cut}} = 10$ truncation, we reach smaller lattice spacings and recover the consistency with the analytical results (blue circles).

launched by the State of Hessen. H.S. was supported by the Japan Society for the Promotion of Science for Young Scientists. We are grateful to the computer centers of DESY Zeuthen, RZG Garching and the Center for Scientific Computing of the Goethe-University in Frankfurt (the LOEWE system) for their computing resources and support.

[1] T. Byrnes, P. Sriganesh, R. Bursill, and C. Hamer, Phys.Rev. **D66**, 013002 (2002), hep-lat/0202014.
[2] K. Cichy, A. Kujawa-Cichy, and M. Szyniszewski, Comput.Phys.Commun. **184**, 1666 (2013), 1211.6393.
[3] M. Bañuls, K. Cichy, K. Jansen, and J. Cirac, JHEP **1311**, 158 (2013), 1305.3765.
[4] M. C. Bañuls, K. Cichy, J. I. Cirac, K. Jansen, and H. Saito, PoS **LATTICE2013**, 332 (2014), 1310.4118.
[5] B. Buyens, K. Van Acoleyen, J. Haegeman, and F. Verstraete, (2014), 1411.0020.
[6] B. Buyens, J. Haegeman, K. Van Acoleyen, H. Verschelde, and F. Verstraete, Phys.Rev.Lett. **113**, 091601 (2014), 1312.6654.
[7] E. Rico, T. Pichler, M. Dalmonte, P. Zoller, and S. Montangero, Phys.Rev.Lett. **112**, 201601 (2014), 1312.3127.
[8] P. Silvi, E. Rico, T. Calarco, and S. Montangero, New J.Phys. **16**, 103015 (2014), 1404.7439.
[9] Y. Shimizu and Y. Kuramashi, Phys. Rev. D **90**, 014508 (2014).
[10] Y. Shimizu and Y. Kuramashi, Phys.Rev. **D90**, 074503 (2014), 1408.0897.
[11] L. Tagliacozzo, A. Celi, and M. Lewenstein, Phys.Rev. **X4**, 041024 (2014), 1405.4811.
[12] J. Haegeman, K. Van Acoleyen, N. Schuch, J. I. Cirac, and F. Verstraete, Phys. Rev. X **5**, 011024 (2015).
[13] S. Borsanyi, G. Endrodi, Z. Fodor, S. Katz, and K. Szabo, JHEP **1207**, 056 (2012), 1204.6184.
[14] U. Heinz *et al.*, Exploring the properties of the phases of QCD matter - research opportunities and priorities for the next decade, 2015, 1501.06477.
[15] I. Sachs and A. Wipf, Helv.Phys.Acta **65**, 652 (1992), 1005.1822.
[16] H. Saito, M. C. Bañuls, K. Cichy, J. I. Cirac, and K. Jansen, PoS **LATTICE2014**, 302 (2014), 1412.0596.
[17] J. Schwinger, Phys. Rev. **128**, 2425 (1962).
[18] J. Kogut and L. Susskind, Phys. Rev. D **11**, 395 (1975).
[19] T. Banks, L. Susskind, and J. B. Kogut, Phys.Rev. **D13**, 1043 (1976).
[20] C. J. Hamer, Z. Weihong, and J. Oitmaa, Physical Review D **56**, 55 (1997), hep-lat/9701015.
[21] F. Verstraete, D. Porras, and J. I. Cirac, Phys. Rev. Lett. **93**, 227205 (2004), cond-mat/0404706.
[22] G. Vidal, Phys. Rev. Lett. **93**, 040502 (2004), quant-ph/0310089.
[23] D. Perez-García, F. Verstraete, M. M. Wolf, and J. I. Cirac, Quantum Inf. Comput. **7**, 401 (2007), quant-ph/0608197.
[24] M. B. Hastings, J. Stat. Mech. **2007**, P08024 (2007).
[25] U. Schollwöck, Annals of Physics **326**, 96 (2011), 1008.3477.
[26] F. Verstraete, J. J. García-Ripoll, and J. I. Cirac, Phys. Rev. Lett. **93**, 207204 (2004), cond-mat/0406426.
[27] M. Zwolak and G. Vidal, Phys. Rev. Lett. **93**, 207205 (2004).
[28] B. Pirvu, V. Murg, J. I. Cirac, and F. Verstraete, New Journal of Physics **12**, 025012 (2010), 0804.3976.
[29] M. Hastings, Phys. Rev. B **73**, 085115 (2006).
[30] A. Molnar, N. Schuch, F. Verstraete, and J. I. Cirac, Phys. Rev. B **91**, 045138 (2015).
[31] M. C. Bañuls, K. Cichy, J. I. Cirac, K. Jansen, and H. Saito.
[32] B. Buyens, private communication.
[33] M.-D. Choi, Linear Algebra and its Applications **10**, 285 (1975).
[34] F. Verstraete, V. Murg, and J. Cirac, Advances in Physics **57**, 143 (2008), 0907.2796.
[35] Notice that this is equivalent to the purification ansatz.
[36] By using symmetric tensors that enforce Gauss' law, the squaring of local bosonic dimensions can nevertheless be avoided [32].
[37] For the smallest $g\beta \leq 0.5$, we use $x \geq 100$, for $0.5 < g\beta \leq 1.5$, $x \geq 100$, and for larger $g\beta$, $x \geq 9$.

Numerical method

For completeness, we describe here the details of the numerical method used in the paper.

To describe the thermal equilibrium state we use the MPO ansatz [26–28],

$$\hat{O} = \sum_{\{i_k, j_k\}} \operatorname{tr}\left(M_0^{i_0 j_0} \cdots M_{N-1}^{i_{N-1} j_{N-1}}\right) |i_0 \cdots i_{N-1}\rangle \langle j_0 \cdots j_{N-1}| \,. \quad (4)$$

The thermal density operator can be written as imaginary evolution of the identity operator [26], $\rho(\beta) \propto e^{-\beta H} = e^{-\frac{\beta}{2}H} \mathbb{1} e^{-\frac{\beta}{2}H}$. By applying a Choi isomorphism [33], $|i\rangle\langle j| \to |i\rangle \otimes |j\rangle$, the operators can be vectorized. The thermal state can thus be approximated as an MPS, by applying the imaginary time evolution operator corresponding to $\tilde{H} = H \otimes \mathbb{1} + \mathbb{1} \otimes H^T$ on the initial vectorized identity (see Fig. 6). As shown in Eq. (1), the Hamiltonian contains non-commutative terms, so we approximate the exponential operator as a sequence of

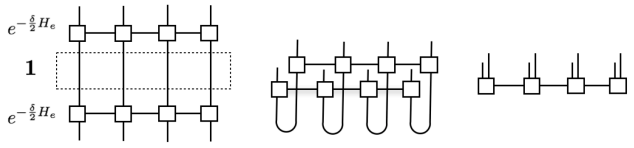

FIG. 6: Schematic representation of the TN operations. Left: applying the first exponential for the first step of imaginary time evolution on the identity operator (which is an MPO with $D = 1$). Center: vectorizing this first step allows us to work with the MPS formalism. Right: after each application of the exponential, the result is approximated by an MPS with bounded bond dimension.

MPOs, to be applied on the MPS. To this end, we use a 2nd-order Suzuki-Trotter expansion,

$$e^{-\beta\tilde{H}} \approx \left[e^{-\frac{\delta}{2}\tilde{H}_e} e^{-\frac{\delta}{2}\tilde{H}_z} e^{-\delta\tilde{H}_o} e^{-\frac{\delta}{2}\tilde{H}_z} e^{-\frac{\delta}{2}\tilde{H}_e}\right]^M. \quad (5)$$

Each evolution step is thus approximated as the successive action of five terms. The exponentials of the hopping terms, $H_{e(o)} = \sum_{n\ \mathrm{even(odd)}}(\sigma_n^+\sigma_{n+1}^- + h.c.)$, have a simple exact MPO expression with maximal bond dimension 4 [28], constructed as simply the product of the individual exponentials of the mutually commuting two-body terms. The remaining term,

$$\begin{aligned} H_z \;=\; & \frac{\mu}{2}\sum_{n=0}^{N-1}[1+(-1)^n\sigma_n^z] \\ & +\frac{1}{4}\sum_{n=0}^{N-2}\left[(n+1)+2\sum_{k=0}^{n}\sum_{l<k}\sigma_k^z\sigma_l^z\right] \\ & +\sum_{\substack{n=0\\(even)}}^{N-2}\left(1+2\sum_{k=0}^{n}\sigma_k^z\right), \end{aligned} \quad (6)$$

contains long-range terms $\sigma_n^z\sigma_m^z$, and, although all terms commute with each other, the product of individual exponentials would yield a bond dimension exponentially large with the system size, N.

A more efficient expression for the exponential exists with bond dimension that only scales linearly in N. We can indeed write H_z as a sum of mutually commuting *local* terms, $H_z = \sum_n h_n$, where, for $n < N-1$,

$$h_n = \frac{\mu}{2}[1+(-1)^n\sigma_n^z] + L_n^2, \quad (7)$$

and $h_{N-1} = \frac{\mu}{2}\left[1+(-1)^{N-1}\sigma_{N-1}^z\right]$, L_n being the electric flux on each link. The exponential of H_z is diagonal in the z spin basis, and its value on a basis vector can be written as a product of the exponentials of each of these terms for the corresponding state. Since the value of L_n, by virtue of Gauss' law, is completely determined by the spin content on sites $k <= n$, the factor corresponding to a given link can be determined from the total magnetization, $\sum_{k\le n}\sigma_k^z$, to the left of the corresponding site. Such information can be encoded in the virtual index of an MPO, which, in a chain of length N, could in principle assume values $L_n \in [-N/2, N/2]$. The exponential can thus be written exactly as an MPO determined by tensors M_n whose only non-vanishing elements are $(M_n^{ii})_{L_{n-1}L_n} = e^{-\delta h_n}$ for $L_n = L_{n-1} + \frac{1}{2}[(-1)^n + (\sigma_n^z)_{ii}]$.

Such exact expression produces an MPO with bond dimension $\mathcal{O}(N)$, which is not practical for the long chains involved in our study. Thus, it is convenient to truncate the MPO by allowing L_n, i.e. the virtual index, to assume only bounded values $|L_n| \le L_{\mathrm{cut}}$, so that the maximum bond dimension is $2L_{\mathrm{cut}} + 1$. This corresponds to a truncation of the physical space to only those spin configurations for which all links have small enough electric flux, since the rest will be projected out when multiplying by the truncated exponential.

Another, more economical approximation to the exponential of H_z can be achieved by a 1st-order Taylor expansion, which can be written as an MPO with bond dimension 3. In this approach, the whole physical space is kept, so that no extrapolation in the L_{cut} parameter is required. In our calculation, we use both approaches.

The exponentials in (5) involve $\tilde{H}_\alpha = H_\alpha \otimes \mathbb{1} + \mathbb{1} \otimes H_\alpha^T$ for each $\alpha = e, o, z$. But since both terms in each $\tilde{H}_\alpha$ commute, the corresponding exponential is just the tensor product of two exponentials, which can then be applied sequentially or simultaneously. After every factor in (5) is written or approximated as an MPO, the effect of one evolution step on a certain intermediate state, vectorized as an MPS, can be approximated as a new MPS with the desired bond dimension. This is achieved by a global optimization (see e.g. [34] for algorithmic details), in which the Euclidean distance $\epsilon = \||\rho'\rangle - O|\rho\rangle\|^2$ between the new MPS, $|\rho'\rangle$, and the result of the operator O on the original one, $|\rho\rangle$, is minimized by successively varying each one of the tensors, and sweeping over the chain until convergence (Fig. 6).